AFRL-RH-WP-TR-2007-0108

RADAR Imaging Transformation for Heads Up Display Utility

Brian Wilson
Nikola Subotic

**Altarum Institute
3520 Green Court
Ann Arbor MI 48105**

September 2007

Final Report for August 2005 to August 2006

**Air Force Research Laboratory
Human Effectiveness Directorate
Warfighter Interface Division
System Control Interfaces Branch
Wright-Patterson AFB OH 45433**

NOTICE

Using Government drawings, specifications, or other data included in this document for any purpose other than Government procurement does not in any way obligate the U.S. Government. The fact that the Government formulated or supplied the drawings, specifications, or other data does not license the holder or any other person or corporation; or convey any rights or permission to manufacture, use, or sell any patented invention that may relate to them.

This report was cleared for public release by the 88th Air Base Wing Public Affairs Office and is available to the general public, including foreign nationals. Copies may be obtained from the Defense Technical Information Center (DTIC) (http://www.dtic.mil).

TECHNICAL REVIEW AND APPROVAL

AFRL-RH-WP-TR-2007-0108

THIS TECHNICAL REPORT HAS BEEN REVIEWED AND IS APPROVED FOR PUBLICATION.

FOR THE DIRECTOR

//signed//
Brian H. Tsou, Ph.D.
Program Manager
System Control Interfaces Branch

//signed//
Daniel G. Goddard
Chief, Warfighter Interfaces Division
Human Effectiveness Directorate

This report is published in the interest of scientific and technical information exchange, and its publication does not constitute the Government's approval or disapproval of its ideas or findings.

REPORT DOCUMENTATION PAGE

1. REPORT DATE *(DD-MM-YYYY)* 01 Sep 2007	2. REPORT TYPE Final	3. DATES COVERED *(From - To)* August 2005 – August 2006

4. TITLE AND SUBTITLE RADAR Imaging Transformation for Heads Up Display Utility	5a. CONTRACT NUMBER FA8650-05-C-6635
	5b. GRANT NUMBER
	5c. PROGRAM ELEMENT NUMBER 62202F
6. AUTHOR(S) Brian Wilson Nikola Subotic	5d. PROJECT NUMBER 7184
	5e. TASK NUMBER 09
	5f. WORK UNIT NUMBER 15

7. PERFORMING ORGANIZATION NAME(S) AND ADDRESS(ES) Altarum Institute 3520 Green Court Ann Arbor MI 48105	8. PERFORMING ORGANIZATION REPORT NUMBER

9. SPONSORING/MONITORING AGENCY NAME(S) AND ADDRESS(ES) Air Force Materiel Command Air Force Research Laboratory Human Effectiveness Directorate Warfighter Interface Division System Control Interfaces Branch Wright-Patterson AFB OH 45433	10. SPONSOR/MONITOR'S ACRONYM(S) AFRL/RHCI
	11. SPONSORING/MONITORING AGENCY REPORT NUMBER AFRL-RH-WP-TR-2007-0108

12. DISTRIBUTION AVAILABILITY STATEMENT
Approved for public release; distribution unlimited.

13. SUPPLEMENTARY NOTES
88th ABW/PA cleared 09 October 2007, WPAFB-07-0045.

14. ABSTRACT
The following report discusses the display and sensor requirements for a heads up display (HUD) capable of presenting a 3-Dimensional (3-D) scene to a pilot during instrument landing that provides data indicative of barriers and obscurations in the flight path and intended landing area. The necessary equations for relating common electro-optic sensor parameters to the equivalent RADAR parameterization are provided such that a cross-sensor analysis can be performed to determine the appropriate sensor data transformations for display. Formulations of the appropriate data transformations are made such that RADAR data can de displayed appropriately such that a human looking through a HUD can easily interpret the RADAR data to provide a 3-D view of the intended landing area.

15. SUBJECT TERMS
Optical Detection, Radar Detection

16. SECURITY CLASSIFICATION OF: **Unclassified**			17. LIMITATION OF ABSTRACT	18. NUMBER OF PAGES	19a. NAME OF RESPONSIBLE PERSON Brian H. Tsou
a. REPORT U	b. ABSTRACT U	c. THIS PAGE U	SAR	26	19b. TELEPONE NUMBER *(Include area code)*

(THIS PAGE INTENTIONALLY BLANK)

Table of Contents

List of Figures

THIS PAGE INTENTIONALLY LEFT BLANK

1   Summary

Providing pilots with a heads up display (HUD) capable of presenting a 3-Dimensional (3-D) scene to a pilot during instrument landing would be beneficial for spontaneous night landings in unknown locations. Remote sensing via RADAR has the opportunity to provide data that fulfills this capability. The HUD would be used to display information about barriers and obscurations in the flight path and intended landing area.

This report covers the transformation and sensor requirements necessary for RADAR imagery to appear in the same geometry as an equivalent optical image; what the pilot sees. Spatial resolution, slant-range to ground-range transformations, and maximum detectable range are covered. Appendices are provided which contain more information on interferometric synthetic aperture RADAR (IFSAR) and an approach for removing terrain artifacts from the data transformations.

2   Introduction

The overall goal of the "RADAR Imaging Transformation for Heads Up Display" study is to explore ways in which a pilot could perform an instrument only landing using RADAR images as the main source of information. RADAR can be used in most types of weather and during night landings, making it a logical choice for spontaneous landing of aircraft. The RADAR data must be displayed in a manner that is consistent with how a pilot looks out of a cockpit. The geometry of the display must be the same as the geometry of the real world through the human visual system.

RADAR data collections take place in a range-angle geometry, as RADAR is typically used as measure of distance. Optical images are collected using an angle-angle geometry, and therefore a transformation is needed to convert RADAR imagery into its equivalent optical image. This report serves to defining sensor requirements, relate electro-optic sensor parameters to the equivalent RADAR parameters, and formulate the data transformations for appropriate display of RADAR imagery.

3   Assumptions

3.1   Flat Earth Assumption in RADAR

The flat Earth assumption used in RADAR is made because normally the radius of Earth is much larger than the distance to the target. The assumption states that the affect of the spherical shape of Earth is insignificant when one is close to the surface of Earth. The parameters below describe the landing scenario used throughout this study, with Figure 1 shown to help guide the derivation of the measurement error. The difference in straight-line distance to the runway, $R_{\mathrm{max\_meas}}$ or R_r, and arc length along the curvature of the Earth, R_{arc}, determines the possible error in measurement.
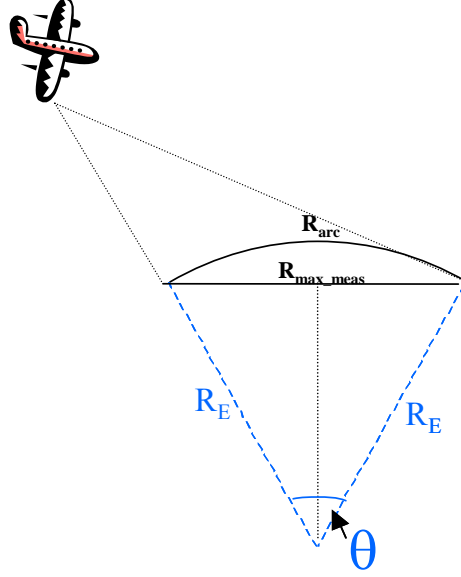
Figure 1: The geometry used for deriving the error inherent in using the flat earth assumption

Based on the above geometry, the angle, θ, can be calculated as shown in equation (1). Once θ is known, arc length can be calculated using equation (2).

$$\sin\left(\frac{\theta}{2}\right) = \frac{R_r/2}{R_E}$$

$$\therefore \theta = 2\sin^{-1}\left(\frac{R_r}{2R_E}\right)$$

(1)

$$R_{arc} = \theta\, R_E$$

(2)

Given the radius of Earth, R_E, as 6371 km and the range to the runway, R_r, as 1.635 km, the measurement error can be calculated to be 4.48 µm, as shown below.

$$\theta = 0.0147^\circ$$

$$\theta = 2.56 \times 10^{-4}\ \text{rad}$$

$$R_{arc} = \theta\, R_E$$

$$R_{arc} = 1.63500000448\text{km}$$

$$R_{arc} = 1.63500000\,448\,\text{km}$$

$$R_r = 1.635\,\text{km}$$

$$\Delta R = R_{arc} - R_r = 4.48\,\mu\text{m}$$

As can be seen from the above calculation, for the parameters given, the flat Earth assumption is valid. The difference in the range to the runway between straight line distance and arc length is 4.5um. Note that this discussion pertains to the curvature of Earth, and not to terrain models. Terrain models are discussed in Appendix C.

4   RADAR and EO Sensor Similarities and Differences

The following discussion covers the differences between electro-optics (EO) sensors and RADAR sensors, specifically in the areas of data collection style and spatial resolution. In order to better transform the RADAR image to its optical equivalent, height information needs to be taken into account. Interferometric synthetic aperture RADAR (IFSAR), can be used to estimate the heights of objects within a scene and is discussed. The maximum detectable range of a RADAR system is also explored.

4.1   RADAR Mode Definitions

The transformation from a RADAR geometry to an EO geometry can be described in terms of a B-scope to C-scope conversion. The B-scope, as shown in Figure 2, displays an image in range and azimuth, the native form of RADAR imagery. A C-scope image has undergone a perspective transformation and appears as an EO image would appear to a pilot. The difficulty in this transformation comes in correctly relaying height information in the C-scope image.
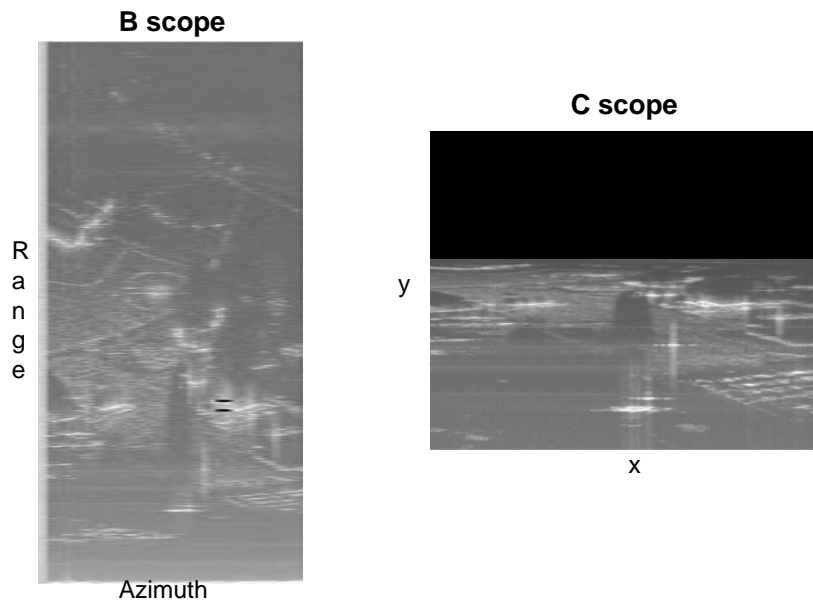

Figure 2: An example of B-scope imagery and C-scope imagery

4.2 Collection Differences

The collection geometry of RADAR systems differs from the geometry of electro-optical systems. Electro-optics data is collected such that pixels are arranged on a Cartesian grid. Pixel location within the grid is determined by noting two angles; azimuth angle α_1 and depression angle α_2, as shown in Figure 3, in order to locate the point along line L_1. Due to this setup, optical systems can also be referred to as angle-angle systems. The disadvantage of an angle-angle system is that an object must be observed from two positions in order to image in three dimensions.

Pixel size and quantization determine the image quality and are dependant upon the imaging hardware.
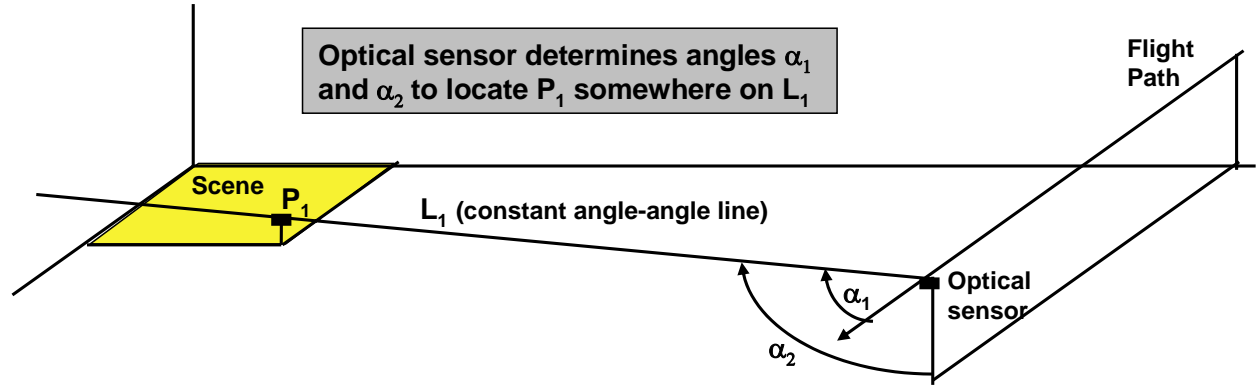
Figure 3: Optical Angle-Angle Positioning of Scatterer P₁

RADAR systems create images by calculating the range to an object and noting the angle in azimuth and depression of the receiver relative to a fixed reference point. This range-angle geometry allows for three dimensional imaging from a single observation point. Range bins exist as concentric circles about the receiver, Due to this geometry, interpolation is necessary in order to view the RADAR pixels correctly on a Cartesian grid. Figure 4 demonstrates the collection geometry of a RADAR system, in this case a system used for synthetic aperture RADAR (SAR). Point P_1 is identified by its location in the circular range bin C_1 by the range R_t and α_d, the angle between the sensor path and P_1.

4
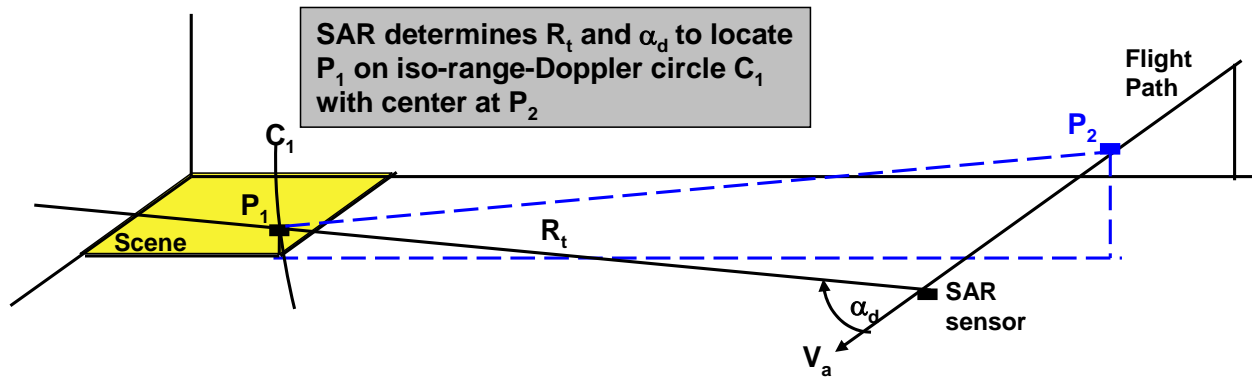
Figure 4: SAR Range-Doppler Positioning of Scatterer P1

A comparison of the angle-angle geometry of EO and the range-angle geometry of RADAR can be seen in Figure 5. An EO image provides intensity information about a single plane within the scene, as each point in the plane can be referenced by its depression angle and azimuth angle. Information about the distance of a point from the reference point cannot be directly obtained. RADAR systems inherently detect range, therefore a point's location along the dotted lines in Figure 5 is provided along with the point's coordinates in azimuth and depression angle. Therefore, the advantage of the range-angle geometry is the ability to obtain three-dimensional information (depression angle, azimuth angle, and range) from a single reference point.

Figure 5: RADAR imagery provides an extra dimension of information over EO imagery

4.3 Spatial Resolution

Spatial resolution determines how well one can distinguish features in an image. In both optics and scanning RADAR, spatial resolution is dependant on frequency and the dimensions of the equipment used for signal detection.

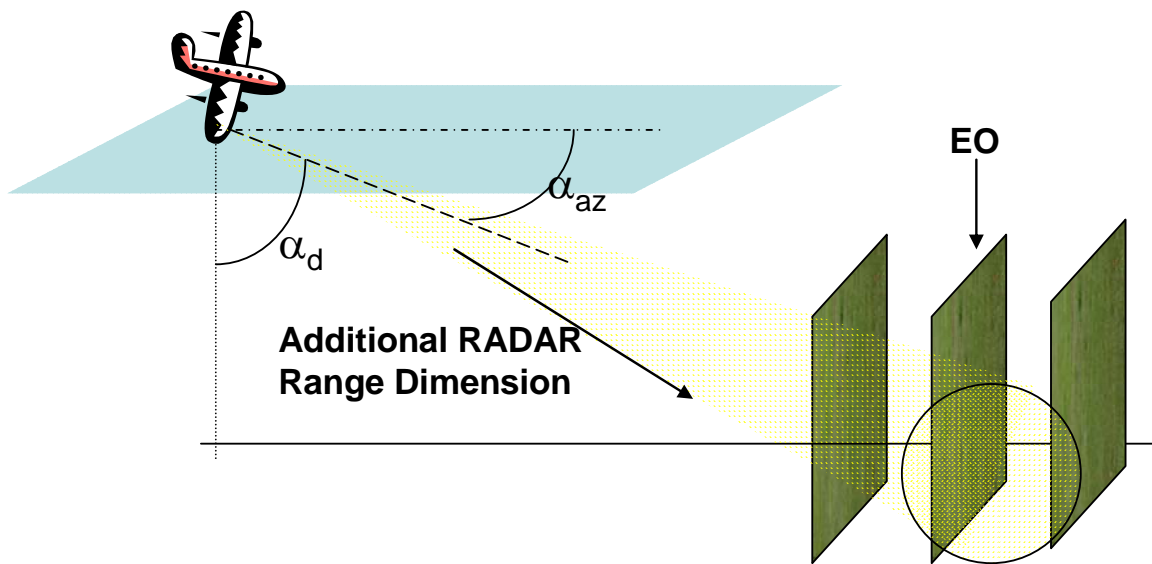The spatial resolution for optics shown in equation (3) relies upon Rayleigh resolution criteria with the diffraction of light as the limiting factor. This equation assumes a spherical lens system; therefore the resolution in both of the cross-range dimensions is the same.

$$\rho = 1.22 \frac{\lambda d_i}{D}$$

λ = wavelength (3)
d_i = distance from lens to image
D = diameter of aperture

Due to the nature of RADAR collections, spatial resolution is specified in both range and cross range. Cross range resolution in RADAR, as shown in equation (4), is similar to the optical resolution of equation (3). Both equations are dependant on wavelength, distance from sensor to target, and the main dimension of the detecting hardware.

$$\rho_{az} = \beta R = \frac{\lambda}{D} R$$

β = beamwidth (4)
λ = wavelength
R = range
D = antenna dimension

Range resolution in scanning RADAR is a function of the pulse length of the RADAR sensor, as shown in equation 5. Pulse length and bandwidth have an inverse relationship.

$$\rho_r = \frac{c\tau}{2} = \frac{c}{2B}$$

c = speed of light (5)
τ = pulse length
B = bandwidth

Another form of RADAR imaging, SAR, can provide increased azimuth resolution by combining several collections from a moving platform into a single beam, effectively increasing the antenna

dimension and creating a finer azimuth resolution. Figure 6 shows a comparison of the resolution cell size for scanning RADAR and SAR. The synthetic beamwidth in the SAR case is a result of the processing of several data collects.
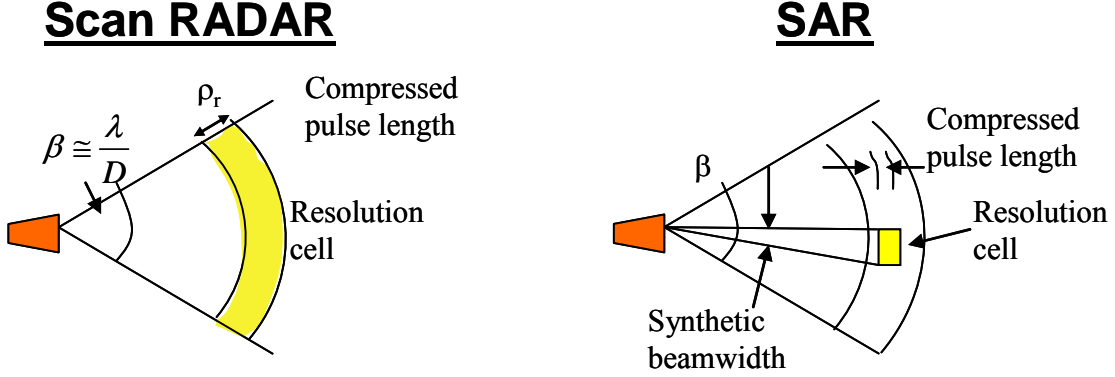
Figure 6: SAR processing allows for better resolution than scanning RADAR

Equation (6) and equation (7) show the updated spatial resolution equations when a SAR processing is used. The mainlobe-broadening factors, K_a and K_r, are constants associated with the antenna hardware.

$$\rho_{az} = \frac{\lambda_c K_a}{2\Delta\theta}$$

λ_c = center frequency

K_a = mainlobe - broadening factor

$\Delta\theta$ = coherent integration

      angular interval

(6)

$$\rho_r = \frac{cK_r}{2B}$$

c = speed of light

K_r = mainlobe - broadening factor

B = pulse bandwidth

(7)

4.4 Spatial Frequency Relationship

Another way of interpreting the difference between EO and RADAR is in the spatial frequency domain of the scene. In the spatial frequency domain, an optical image occupies a plane parallel to the f_x-f_y plane shown in Figure 7. Due to the differences in collection geometries stated earlier, SAR data collections fill in the three dimensional space by collecting data around a cone as shown in Figure 7. A two-dimensional cut through this cone shows that a RADAR sensor will fill in only one line in the same plane as an optical sensor.
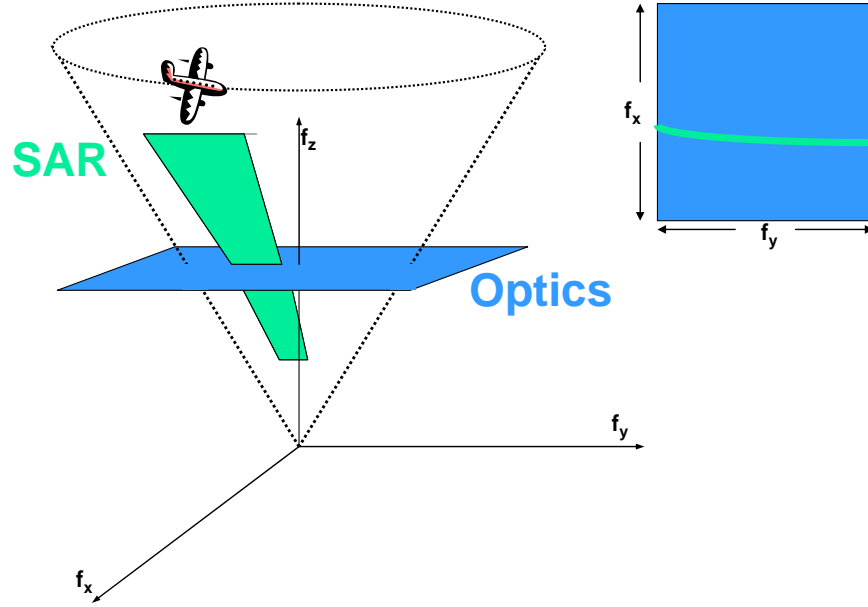
Figure 7: Spatial frequency relationship between an optical sensor and SAR

4.5 Interferometric Synthetic Aperture RADAR (IFSAR)

Interferometric synthetic aperture RADAR (IFSAR) requires the use of two receivers offset from one another by a known amount. This collection geometry allows for the discernment of height information based on the phase differences between the received signals on the two antennas from a single pulse aimed at the same target. A derivation of the height equation, shown in equation (8), can be found in Appendix A. In equation (8), z is the height of an object, h_{ant} is the height of the antennas, and R is the slant range between an antenna and the target. The imaging geometry shown in Figure 8 is representative of the collection geometry for the example data set used in algorithm testing for the overall project.

$$z = h_{ant} - R\cos\theta \quad (m) \tag{8}$$

8

h_{ant} = antenna height = 100 m

B = interferometer baseline = 0.024 m

ρ = range to target = [0...3615.2] m

ξ = approach angle = 3.5º

R = measured slant range
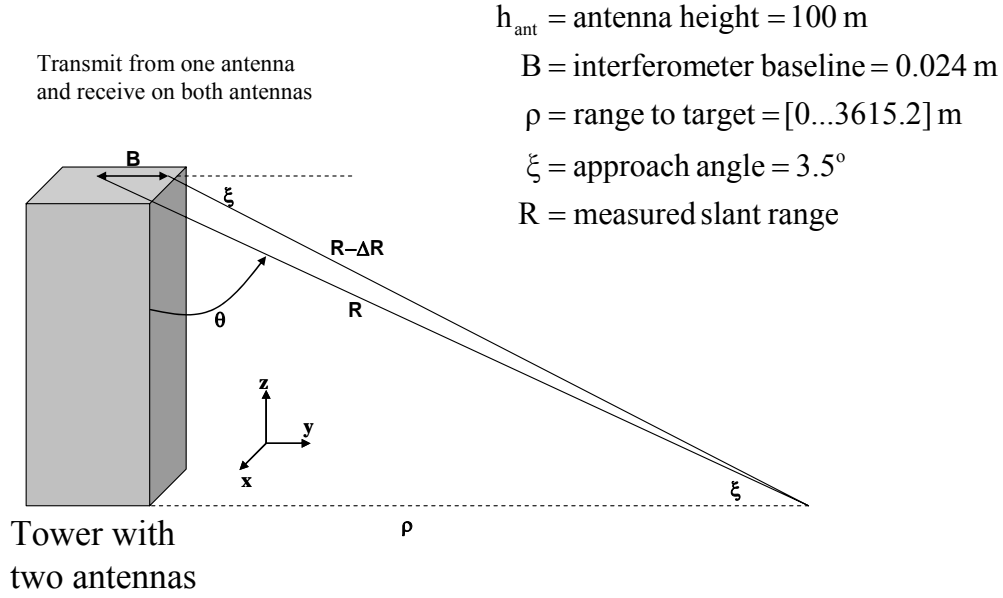
Figure 8: Data Collection Geometry used in this study for algorithm development

4.6 *Slant Range to Ground Range Transformation*

Slant range to ground range distortion in RADAR imagery occurs because the RADAR is measuring distance along the slant-range as opposed to the true horizontal ground distance to a target. As shown in the right side of Figure 9, this causes targets in the near range to appear compressed relative to the far range.

A projection operator such as the one in equation (9) can be used to convert slant plane imagery into ground plane imagery.

$$GRI = \text{proj}_{\vec{R}_G} \vec{R}_S = \frac{\vec{R}_G \bullet \vec{R}_S}{\left|\vec{R}_G\right|^2} \vec{R}_G \qquad (9)$$

Figure 9: Slant range to ground range conversion geometry with associated imaging artifacts

4.7 Maximum Detectable Sensor Range

The hardware of a RADAR system determines the maximum detectable range for a given target signal-to-noise ratio (SNR). This maximum detectable rang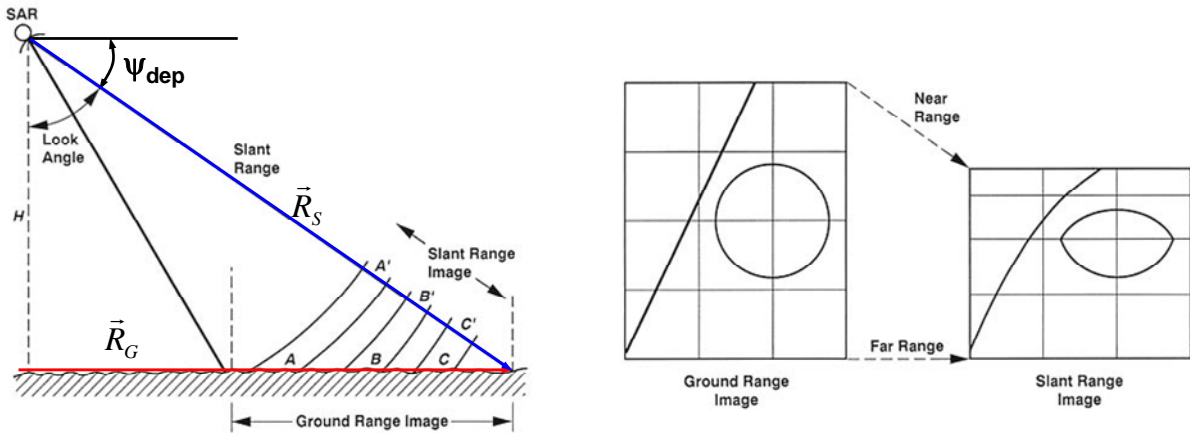e is analogous to the horizon of an optical image, which is limited by the curvature of Earth. Because a RADAR sensor is its own source, the RADAR horizon can be defined as the minimum of the detectable range due to geometry and detectable range due to the output power of the RADAR transmitter for a given SNR.

Appendix B contains a short primer on the basic RADAR equations necessary to construct an estimate for the maximum detectable sensor range based on parameters used in this study. The derivation for this equation also necessitates a description of the RADAR cross section of a planar target, which is contained in section 4.7.2.

4.7.1 Maximum Detectable Range Due to Collection Geometry

A good estimate for the geometric RADAR horizon is provided in the *Naval Electronic Warfare and RADAR Systems Engineering Handbook* and is shown in equation (10). The value $\frac{4}{3}$ is an empirical value used to estimate the wave distortion of the atmosphere, R_E is the radius of Earth, and h_{ant} is the height of the antenna.

$$R_{max} = \sqrt{2 \cdot \frac{4}{3} \cdot R_E \cdot h_{ant}} \quad (m) \tag{10}$$

4.7.2 RADAR Cross Section for Planar Target

The RADAR cross section (RCS) of an object is a measure of how an object reflects an incident electromagnetic wave. When trying to calculate the distance to the RADAR horizon, there is not one specific object reflecting energy, as the Earth's surface as a whole must be taken into account. This can be done if the Earth's surface is treated as distributed clutter over a planar target. The RCS, σ_t, of the Earth's surface is defined by the back-scatter coefficient of distributed ground clutter and the resolution cell of the RADAR as shown in equation (11). Figure 10 shows the geometry for this scenario.

$$\sigma_t = \rho_r \cdot \rho_{az} \cdot \sigma_{bs} \; (m^2) \tag{11}$$
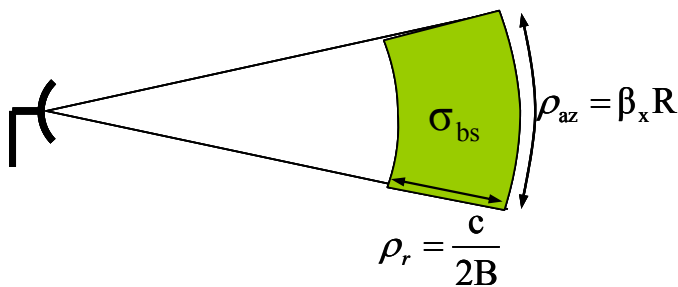
ρ_r = range resolution (m)
ρ_{az} = azimuth resolution (m)
σ_{bs} = back-scatter coeff. (unitless)
β_x = beamwidth (rad)
R = range (m)
B = bandwidth (Hz)

$\rho_{az} = \beta_x R$

$\rho_r = \dfrac{c}{2B}$

Figure 10: Geometry for calculating the RCS of a planar target

The backscatter coefficient of distributed clutter depends on the angle of incidence and has been previously measured by Gatesman, et al, as shown in Figure 11.
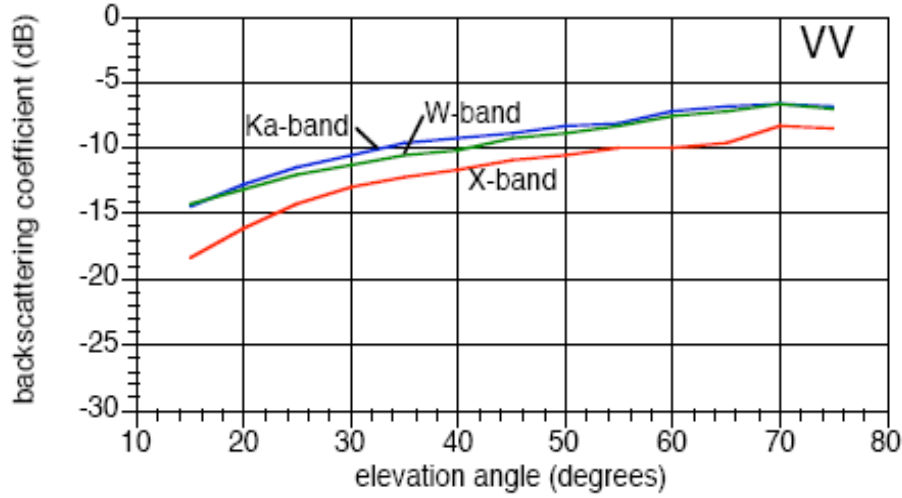

Figure 11: Back scattering coefficient for distributed ground clutter

4.7.3   Maximum Detectable Range Due to Transmitter Power

RADAR range depends on transmitter power because a RADAR is its own source. The maximum range for a given transmit power can be found by solving the standard RADAR equation, equation (12) for range.

$$P_r = \frac{P_t G_t G_r \lambda^2 G_p \sigma_t}{(4\pi)^3 R_t^2 R_r^2}$$

(12)

Assuming a monostatic collection geometry and replacing σ_t with equation (11), equation (12) becomes:

$$P_r = \left(\frac{P_t G^2 \lambda^2 G_p}{(4\pi)^3 R^4} \right) \left(\frac{c}{2B} \cdot \beta R \cdot \sigma_{bs} \right)$$

(13)

Using the antenna gain definition from Appendix B and solving equation (13) for *R* provides the equation for the maximum detectable RADAR range in terms of transmit power in equation (14).

$$R_{max} = \left[\frac{P_t d_x d_y^2 \xi^2 f_c \sigma_{bs} G_p}{8\pi \cdot B \cdot SNR \cdot P_n} \right]^{1/3}$$

(14)

11

4.7.4 Calculation of RADAR Horizon using given values

The set of parameters in Figure 12 was used in this study for algorithm development.

$$
\begin{aligned}
h_{ant} &= 100\,\text{m} \\
d_x = d_y &= 0.12\,\text{m} \\
\xi &= 0.85 \;\;(\text{typical estimate}) \\
f_c &= 94\,\text{GHz} \\
\sigma_{bs} &= -8\,\text{dB} = 0.16\,(\text{unitless}) \\
G_p &= 16384 = 42\,\text{dB}\,(\text{unitless}) \\
B &= 300\,\text{MHz} \\
SNR &= [20,35,45\,\text{dB}] = [100,3162,31623] \\
P_n &= -111\,\text{dB} = 7.8 \times 10^{-12}\,\text{W}
\end{aligned}
$$

Figure 12 : Given parameters for the RADAR collection used in this study

Using these parameters in equation (10) gives a maximum range due to geometry of 41,260 meters. Solving equation (14) for the maximum range due to transmit power gives a distance of 3722 meters, assuming a transmit power of one Watt and an SNR of 20 dB. Therefore, for this scenario, the RADAR transmit power is the dominant contributor to the overall maximum detectable range. Figure 13 provides the maximum detectable sensor range for this experiment for three values of SNR and a range of transmit powers.
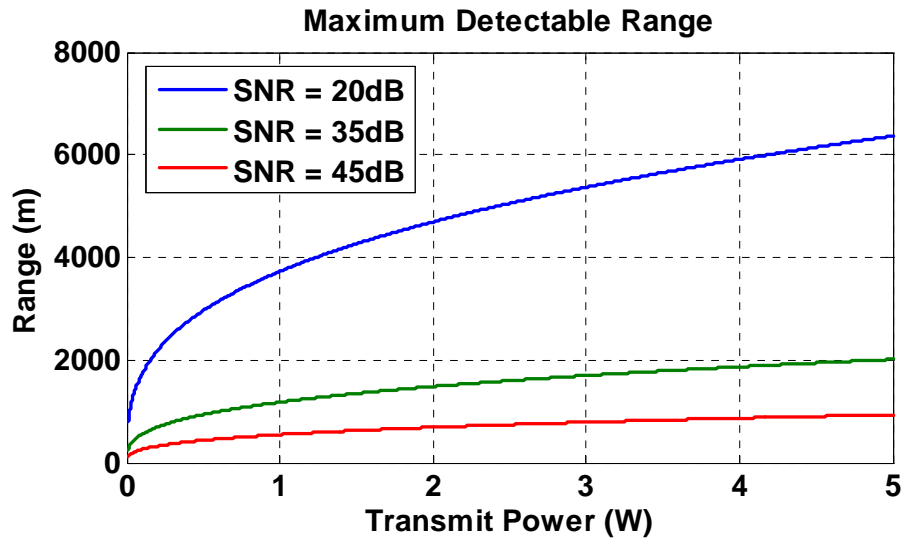

Figure 13 : Maximum detectable range for the scenario in this study

5   Conclusions

The purpose of this report was to examine some of the required RADAR sensor parameters and transformations in order to convert a RADAR image into its equivalent optical image for the purpose of landing an aircraft via a heads up display. Equations for spatial resolution, slant range to ground range transformation, and maximum sensing distance were presented.

Concern over adjusting for the underlying terrain of an image could be addressed as shown in Appendix C. Future work on this project could involve furthering the ideas of Appendix C to create an automated way of adjusting for the terrain in an image.

6 Bibliography

1. *ASF SAR Processing Algorithm*:
   http://www.asf.alaska.edu/reference_documents/datacenters_references/sar_processing.html

2. Carrara, Walter G., et al: Spotlight Synthetic Aperture Radar: Signal Processing Algorithms, Artech House,1995, pp. 21-40

3. Farr, T.G. "Chapter 5: Radar Interactions With Geologic Surfaces:" *Guide to Magellan Image Interpretation*: http://history.nasa.gov/JPL-93-24/ch5.htm

4. Gatesman, et al. "Polarimetric Backscattering Behavior of Ground Clutter at X, Ka, and W-band." Proceedings of SPIE 5808, 428 (2005)

5. Gonzalez, Rafael C. and Richard E. Woods. *Digital Image Processing*. Addison-Wesley, 1993, pp. 53-6.

6. Goodman, J.W. *Introduction to Fourier Optics*, McGraw-Hill, 1968, pp. 130

7. "RADAR HORIZON / LINE OF SIGHT." *Electronic Warfare and RADAR Systems Engineering Handbook.* https://ewhdbks.mugu.navy.mil/rdr-hori.htm

8. Ulaby, Fawwaz T.: *Fundamentals of Applied Electromagnetics*, 1999 Edition, Prentice Hall, 1999, pp. 370-1, 401-4

9. Walker, Jack L. "Range-Doppler Imaging of Rotating Objects". Dissertation. University of Michigan. 1974.

Appendix A - Derivation of Height Equation Using IFSAR

Each pixel in an image contains two data points, one from each of the receive antennas. The two received signals are shown in equation (A1) and equation (A2), with the major difference in the signals being the extra phase term in I_2. The geometry for this derivation is the same as in Figure 8.

$$I_1 = a_1 e^{j\left(\varphi_{R1} + \frac{2\pi}{\lambda}2R\right)}$$
(A1)

$$I_2 = a_2 e^{j\left(\varphi_{R2} + \frac{2\pi}{\lambda}[R+R-\Delta R]\right)}$$
(A2)

If the interferometer spacing B is not too large, the amplitude and phase of the complex reflectivity is nearly the same for each antenna, thus the simplifications $a = a_1 = a_2$ and $\varphi_{R1} = \varphi_{R2}$ can be made.

If we form an interferogram from the images, we have:

$$I_{1,2} = I_1 I_2^*$$
$$= a^2 e^{j\left(\frac{2\pi\Delta R}{\lambda}\right)}$$
$$I_{1,2} = a^2 e^{j\varphi}$$
(A3)

where $\varphi = \dfrac{2\pi\Delta R}{\lambda}$.

The law of cosines, equation (A4), allows us to obtain ΔR by expanding and dropping terms $O(\Delta R^2), O\left(\dfrac{B^2}{R}\right)$. The resulting equations for ΔR, and ultimately φ, are shown in equation (A5) and equation (A6) respectively.

$$(R - \Delta R)^2 = R^2 + B^2 - 2RB\cos\left(\frac{\pi}{2} - \theta + \alpha\right)$$
(A4)

$$\Delta R = B\sin(\theta - \alpha)$$
(A5)

$$\varphi = \frac{2\pi B}{\lambda}\sin(\theta - \alpha)$$
(A6)

Solving for θ shows that if we measure the phase at each image point we can obtain the angular location of the image points. This relationship is explicitly shown in equation (A7).

$$\theta = \sin^{-1}\left(\frac{\lambda\varphi}{2\pi B}\right) + \alpha \qquad\qquad (\text{A7})$$

We can obtain the y and z coordinates of each image point using equation (A8) and equation (A9).

$$y = R\sin\theta \qquad\qquad (\text{A8})$$

$$z = H - R\cos\theta \qquad\qquad (\text{A9})$$

In summary, if α, B, and, H are known, then height of an object, can be calculated from the interferogram, as height is dependant upon θ, which is derived from φ, which is determined by the interferogram.

Appendix B - Basic RADAR Equations

Noise Power

$$P_n = P_{noise} = K \cdot T \cdot F \cdot B$$

$K = 1.38 \times 10^{-23} \text{ W/(Hz} \cdot \text{K)}$

$T = \text{system temperature (K)}$ (B1)

$F = \text{loss factor (unitless, } \sim 8 \text{ dB)}$

$B = \text{bandwidth (Hz)}$

Antenna Beamwidth

$$\beta \cong \frac{\lambda}{d}$$

$\beta = \text{beamwidth (rad)}$ (B2)

$\lambda = \text{wavelength (m)}$

$d = \text{antenna dimension (m)}$

Antenna Gain

$$G \equiv \frac{4\pi \, d_x d_y \xi}{\lambda^2}$$

$d_x = \text{antenna dimension (m)}$ (B3)

$d_y = \text{antenna dimension (m)}$

$\xi = \text{antenna efficiency (unitless)}$

Signal-to-Noise Ratio (SNR)

$$SNR = \frac{P_r}{P_n}$$

$SNR = \text{signal to noise ratio}$ (B4)

$P_r = \text{received power(W)}$

$P_n = \text{noise floor (W)}$
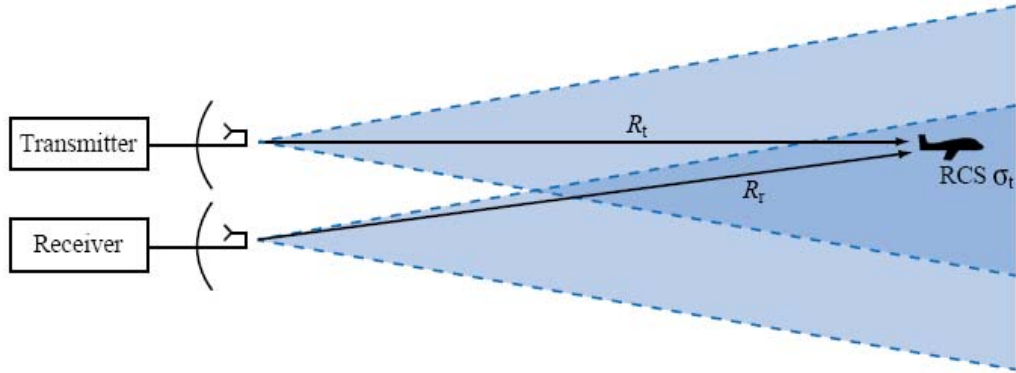
<u>RADAR Equation</u>

Figure B-1: RADAR Equation

$$P_r = \frac{P_t G_t G_r \lambda^2 G_p \sigma_t}{(4\pi)^3 R_t^2 R_r^2}$$

$P_r \equiv$ receiver power (W)

$P_t \equiv$ transmitter power (W)

$G_t \equiv$ antenna gain (unitless)

$G_r \equiv$ antenna gain (unitless)   (B5)

$\lambda \equiv$ wavelength (m)

$G_p \equiv$ range compression processing gain (unitless)

$\sigma_t \equiv$ target RADAR cross section (RCS) (m^2)

$R_t =$ range from antenna to target (m)

$R_r =$ range from target to antenna (m)

Appendix C - Algorithm for Testing Terrain Distortion

A possible extension of this program is to include terrain modeling into the RADAR imagery in order to better mimic the optical imagery. As shown in the SAR geometry, a transformation from slant range to ground range is performed in order to better align an image with its optical counterpart. However, this transformation assumes that the projection is taking place onto a flat ground, which is not true in most cases. A potential way to overcome this problem is shown in Figure C1.
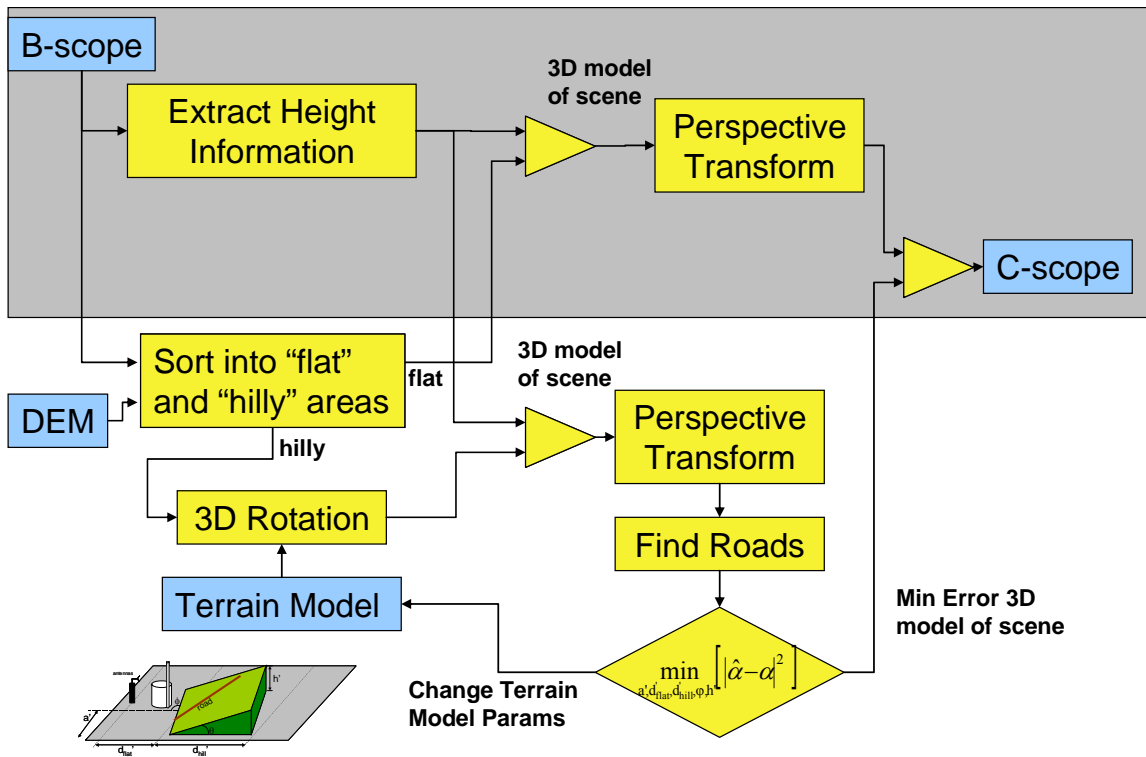

Figure C-1: Overview of algorithm for incorporating local terrain modeling

A Digital Elevation Model (DEM), such as the one in Figure C2, can be used to separate hilly areas of a scene from relatively flat areas of a scene. The threshold for this separation has yet to be determined.
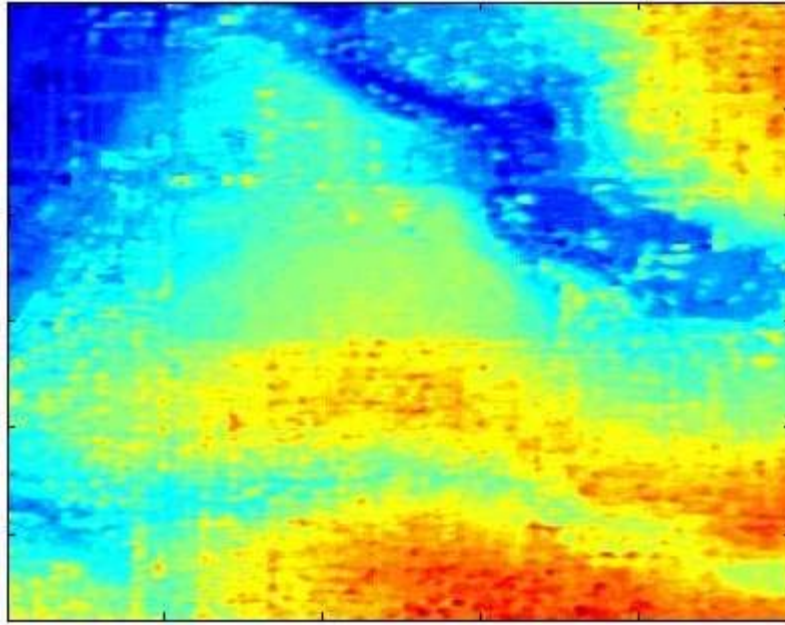
Figure C-2: An example of a Digital Elevation Model (DEM)

The hilly areas of the scene can then be transformed into a series of wedges, one of which is shown in Figure C3. The wedges can then be rotated in three dimensions until a suitable orientation has been found for each wedge.
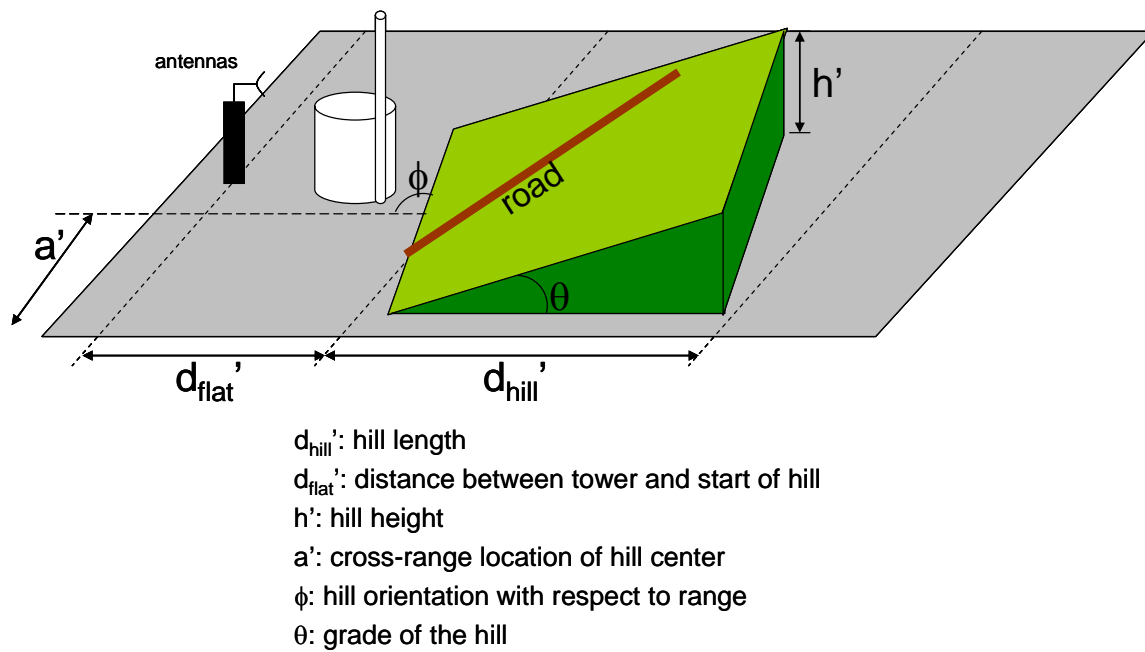

d_{hill}': hill length
d_{flat}': distance between tower and start of hill
h': hill height
a': cross-range location of hill center
ϕ: hill orientation with respect to range
θ: grade of the hill

Figure C-3: One example of a terrain model correction wedge

20

Three dimensional (3-D) rotation algorithms are commonplace in computer graphics rendering engines. An example of the transformation matrices necessary for computing a 3-D rotation are shown in Figure C4. Furthermore, if the object is not located at the origin, the object must first be translated to the point of origin, then rotated, and finally translated back to the objects original location.

$$R_\gamma = \begin{bmatrix} \cos\gamma & \sin\gamma & 0 & 0 \\ -\sin\gamma & \cos\gamma & 0 & 0 \\ 0 & 0 & 1 & 0 \\ 0 & 0 & 0 & 1 \end{bmatrix}$$

$$R_\alpha = \begin{bmatrix} 1 & 0 & 0 & 0 \\ 0 & \cos\alpha & \sin\alpha & 0 \\ 0 & -\sin\alpha & \cos\alpha & 0 \\ 0 & 0 & 0 & 1 \end{bmatrix}$$
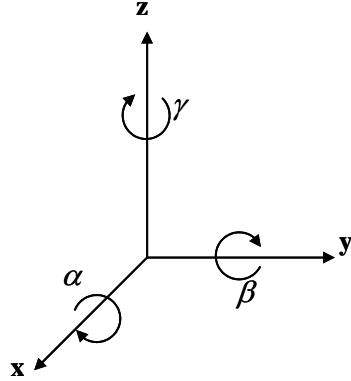
$$R_\beta = \begin{bmatrix} \cos\beta & 0 & -\sin\beta & 0 \\ 0 & 1 & 0 & 0 \\ \sin\beta & 0 & \cos\beta & 0 \\ 0 & 0 & 0 & 1 \end{bmatrix}$$

Figure C-4: Transformation matrices for performing a 3-D rotation

The accuracy of the terrain model would be improved by minimizing the mean squared error between a feature, e.g., a road, in the optical image and an object in the RADAR image. For example, after the road is first extracted from the scene in both the transformed RADAR image and the optical image, the accuracy of the terrain model can be discerned via the squared error between the angle of the road in the RADAR ($\hat{\alpha}$) and optical images (α).

$$\min_{a',d'_{flat},d'_{hill},\varphi,\theta,h'} \left[|\hat{\alpha} - \alpha|^2 \right] \tag{C1}$$

Finally, iterations over various terrain model sizes and orientations can be done until a sufficiently small error is found.